The Src Homology and Collagen A (ShcA) adaptor protein is required for the spatial organization of the costamere/Z-disk network during heart development.

Mlih, M. and Host, L. and Martin, S. and Niederhoffer, N. and Monassier, L. and Terrand, J. and Messaddeq, N. and Radke, M. and Gotthardt, M. and Bruban, V. and Kober, F. and Bernard, M. and Canet-Soulas, E. and Abt-Jijon, F. and Boucher, P. and Matz, R.L.

Journal of Biological Chemistry
2015 JAN 23 ; 290(4): 2419-2430
Doi: 10.1074/jbc.M114.597377

American Society for Biochemistry and Molecular Biology

THE JOURNAL OF BIOLOGICAL CHEMISTRY VOL. 290, NO. 4, pp. 2419–2430, January 23, 2015

The Src Homology and Collagen A (ShcA) Adaptor Protein Is Required for the Spatial Organization of the Costamere/Z-disk Network during Heart Development*[S]

Received for publication, July 16, 2014, and in revised form, December 5, 2014 Published, JBC Papers in Press, December 8, 2014, DOI 10.1074/jbc.M114.597377

Mohamed Mlih[‡1], Lionel Host[‡1], Sophie Martin[‡], Nathalie Niederhoffer[§], Laurent Monassier[§], Jérôme Terrand[‡], Nadia Messaddeq[¶], Michael Radke[‖], Michael Gotthardt[‖**], Véronique Bruban[‡], Frank Kober[‡‡], Monique Bernard[‡‡], Emmanuelle Canet-Soulas[§§], Francisco Abt-Jijon[‡], Philippe Boucher[‡2,3], and Rachel L. Matz[‡2,4]**

*From the [‡]CNRS, UMR 7213, University of Strasbourg, 67401 Illkirch, France, the [§]Laboratory of Neurobiology and Cardiovascular Pharmacology Department, EA 7296, Federation of Translational Medicine, University of Strasbourg, 67000 Strasbourg, France, the [¶]IGBMC, INSERM U964 CNRS UMR 7104, University of Strasbourg, 67401 Illkirch, France, the [‖]Neuromuscular and Cardiovascular Cell Biology, Max-Delbrück-Center for Molecular Medicine, 13125 Berlin, Germany, the **DZHK, German Centre for Cardiovascular Research, partner site, 13347 Berlin, Germany, the [‡‡]CRMBM, CNRS, UMR 7339, University of Aix-Marseille, 13385 Marseille, France, and the [§§]CREATIS-LRMN, CNRS, UMR 5220, U630 INSERM, 69621 Villeurbanne, Lyon-1 University, Lyon, France*

Background: The Src homology and collagen A (ShcA) adaptor protein plays a crucial role in heart development but the underlying mechanisms are unknown.
Results: Early conditional deletion of ShcA in cardiomyocytes leads to heart failure with abnormalities in the costamere/Z-disk network.
Conclusion: ShcA protects against heart failure by maintaining costameres/Z-disk axis integrity.
Significance: Understanding molecular mechanisms involved in heart failure may help to develop new therapies.

Src homology and collagen A (ShcA) is an adaptor protein that binds to tyrosine kinase receptors. Its germ line deletion is embryonic lethal with abnormal cardiovascular system formation, and its role in cardiovascular development is unknown. To investigate its functional role in cardiovascular development in mice, ShcA was deleted in cardiomyocytes and vascular smooth muscle cells by crossing ShcA flox mice with SM22a-Cre transgenic mice. Conditional mutant mice developed signs of severe dilated cardiomyopathy, myocardial infarctions, and premature death. No evidence of a vascular contribution to the phenotype was observed. Histological analysis of the heart revealed aberrant sarcomeric Z-disk and M-band structures, and misalignments of T-tubules with Z-disks. We find that not only the ErbB3/Neuregulin signaling pathway but also the baroreceptor reflex response, which have been functionally associated, are altered in the mutant mice. We further demonstrate that ShcA interacts with Caveolin-1 and the costameric protein plasma membrane Ca^{2+}/calmodulin-dependent ATPase (PMCA), and that its deletion leads to abnormal dystrophin signaling. Collectively, these results demonstrate that ShcA interacts with crucial proteins and pathways that link Z-disk and costamere.

Heart failure is defined as the inability of the heart to sufficiently pump blood to meet the metabolic demands of the body. It is a progressive and complex pathology usually accompanied by dilated cardiomyopathy. Signaling through Z-disk-associated proteins (1, 2) or pathways involving tyrosine kinase receptors such as ErbB2 receptors in the cardiac T-tubule system are among the mechanisms that cause dilated cardiomyopathies (3, 4).

ShcA[5] is an ubiquitously expressed adaptor protein that binds specific phosphotyrosine (Tyr(P)) sites of tyrosine kinase receptors, such as the platelet-derived growth factor receptor, the insulin-like growth factor receptor, or ErbBs once activated by phosphorylation (5). ShcA also binds to integrins (6). ShcA recruitment to the plasma membrane causes its phosphorylation on tyrosine residues, which, in turn, induces the formation of a stable complex with the adaptor protein Grb2 and the Ras guanine nucleotide exchange factor SOS (5, 7). These events lead to the activation of the Erk/mitogen-activated protein kinase pathway and cell proliferation (5, 8). Germline deletion of ShcA in mice leads to profound embryonic cardiovascular defects (9), whereas deletion of ShcA in cardiomyocytes after birth induces a moderately impaired systolic function (10). Thus, ShcA plays a crucial role during heart development, but the underlying molecular mechanisms are largely unknown.

Costameres are platforms in the plasma membrane that participate in signaling between the extracellular matrix and the Z-disk. Costameres encircle the myocyte perpendicular to its long axis, and are comprised of two protein complexes: the dystrophin-glycoprotein complex (DGC) and the vinculin-talin-integrin system, where ShcA localizes through its interac-

* This work was supported by grants from the Fondation de France, Fondation pour la Recherche Médicale (FRM), and Agence Nationale de la Recherche Grants ANR-06-Physio-032-01 and ANR-09-BLAN-0121-01.
[S] This article contains supplemental Videos S1 and S2.
[1] Both authors are considered co-first authors.
[2] Both authors are considered co-senior authors.
[3] To whom correspondence may be addressed. E-mail: philippe.boucher@unistra.fr.
[4] To whom correspondence may be addressed. Tel.: 33-0-3-6885-4149; Fax: 33-0-3-6885-4313; E-mail: rachel.matz-westphal@unistra.fr.

[5] The abbreviations used are: ShcA, Src homology and collagen A; SM22a, smooth muscle 22 protein; PMCA, plasma membrane calcium/calmodulin-dependent ATPase; DGC, dystrophin-glycoprotein complex; Cav, caveolin; LVEDD, left ventricular cross-sectional internal diameter in end-diastole; LVESD, left ventricular cross-sectional internal diameter in end-systole; MBF, myocardial blood flow; Nrg-1, Neuregulin-1.

tion with integrins. The DGC consists of dystrophin, sarcoglycans, dystroglycans, syntrophins, and sarcospan in the costameres of muscle cells (2). Caveolin-1 (Cav-1) and Caveolin-3 (Cav-3) are the predominant caveolin isoforms in the heart, and are also part of the DGC. Only Cav-1 is required for caveolae formation and has been described to functionally interact with ShcA (11), but both Cav-1 and Cav-3 have been identified as potential regulators of heart disease (12). The cardiomyocyte plasma membrane Ca^{2+}-ATPase (PMCA) that extrudes Ca^{2+} from the cytosol (13) binds to α-syntrophin and NOS-1 in cardiac cells (14), and is thus a part of the dystrophin complex. Interestingly, ShcA induces apoptosis through down-regulation of PMCA, suggesting a functional interaction between ShcA and PMCA (15). Furthermore, PMCA binds to PDZ domain-containing proteins through its C terminus (16) and directly associates with the tumor suppressor Ras-associated factor (RASSF1) to inhibit the Ras/Erk pathway (17), the downstream effector of ShcA. Thus, by functionally interacting with ShcA, PMCA could be a hub for ShcA/Cav-1 and α-syntrophin/NOS-1 in the DGC.

Because the genetic deletion of ShcA in adult mice leads to a moderate cardiac phenotype (10), we reasoned that its deletion in cardiomyocytes during early embryogenesis could lead to structural changes and signaling alterations that may help to understand its role during mouse heart embryonic development. We sought to evaluate this relationship using Cre-loxP technology and the Sm22cre transgene, because Sm22 is already expressed at E8.5 in the heart and will remain expressed in the cardiovascular system throughout adulthood (18, 19). The resulting phenotype was a severe dilated cardiomyopathy with aberrant intercalated disk structures and sudden death after birth. Our data suggest that loss of ShcA activity in the heart leads to abnormal ErbB3 and dystrophin signaling in the costamere/Z-disk axis and provide insight into the molecular mechanisms by which ShcA regulates heart development and function.

EXPERIMENTAL PROCEDURES

Animals and Diets—All animal experimentation and procedures were approved by the Institutional Animal Care and Use Committee (IACUC) of the University of Strasbourg, France. We generated mice with loss of ShcA in cardiovascular tissue, using LoxP-flanked ShcA alleles and the Sm22Cre recombinase transgene (Sm22cre) (20). The 10.1-kb DNA sequence containing the mouse exon 1 to exon 11 segments of ShcA, two loxP sites (flanking exons 2 to 7), and a PKG neomycin resistance cassette flanked by two FRT sites, were cloned into the pBlueScript SK(+) vector (targeting vector). The PKG neomycin resistance cassette was excised by crossing ShcA flox/FRT mice with mice expressing flippase recombinase. The resulting $Sm22Cre^{+}$; $ShcA^{flox/flox}$ mice in which ShcA was ablated in heart are referred to as $smShcA^{-}$, and their age and sex-matched control littermates are referred to as Ctrl ($Sm22Cre^{-}$; $ShcA^{flox/flox}$). In the $smShcA^{-}$ animals, the deleted genomic sequence contains exons 2 to 7, which encodes most of the PTB domain of the ShcA protein. Genotyping of the wild-type floxed and null alleles of ShcA by polymerase chain reaction (PCR) was performed as described (20) using primers specific for ShcA (primers available upon request). For atherogenic studies, mutants and control mice were fed a Paigen diet for 24 weeks as described previously (20).

Echocardiography, Blood Pressure Measurements, and Electron Microscopy—Animals were weighted and analyzed for cardiac anatomy and function on a Sonos 5500 (Hewlett Packard) with a 15 MHz linear transducer (15L6). Mice were anesthetized with isoflurane (2% in O_2), placed on a heating table, and the chest area was depilated. The measurements were performed as previously described (21). The heart was first imaged in the two-dimensional mode in the parasternal long-axis view to obtain the aortic root dimensions. The aortic flow velocity and the heart rate were measured with a pulsed-wave Doppler on the same section. The sample volume cursor was placed in the aortic root and the transducer was angled slightly, which allowed paralleling the aortic flow with the interrogation beam so that the maximum aortic flow velocity was obtained easily. The cardiac output was calculated from the following equation: cardiac output $= 0.785 \times D^2 \times \text{VTI} \times$ heart rate, where D is the internal diameter of the aortic root and VTI is the velocity-time integral of the Doppler aortic spectrum. Left ventricular cross-sectional internal diameters in end-diastole (LVEDD) and in end-systole (LVESD) were obtained by an M-mode analysis of a two-dimensional short axis view at the papillary muscle level. The shortening fraction was calculated as SF = (LVEDD-LVESD/LVEDD) × 100, and the ejection fraction using the equation: ejection fraction = (LVEDV-LVESV/LVEDV) × 100, where LVEDV and LVESV are, respectively, LV end-diastolic and LV end-systolic volumes. From this view, the diastolic septum (S) and posterior wall thicknesses were measured. The left ventricular mass was calculated as described (22, 23). All measurements were performed on at least three beats, according to the guidelines of the American Society of Echography. Fractional shortening and ejection fraction were calculated according to the Teichholz formula (24).

Systolic blood pressure rate was recorded by the tail-cuff method in awake mice (Letica model 5002). Electron microscopy was performed as described (25).

In Vivo Myocardial Perfusion Measurement Using MRI—In vivo magnetic resonance images were acquired using a Bruker Biospec 4.7T/30 imager (Bruker Biospin, Ettlingen, Germany). During the MRI protocol, animals were anesthetized with 1.2–1.6% isoflurane delivered in a 0.6 ml/min oxygen gas stream through a dedicated nose cone. An ECG- and respiration-gated Lock-Locker Gradient Echo Flow-sensitive Alternating Inversion Recovery Arterial Spin Labeling technique setup and validated earlier (26, 27) was used to acquire myocardial blood flow (MBF) maps from a single short-axis slice placed at left ventricular (LV) midlevel. The following parameters were used: field of view 25 × 25 mm^2, spatial resolution 195 × 390 mm^2, slice thickness 1.5 mm. The total MBF acquisition time was ~25 min. Perfusion raw images were post-processed as described earlier (26, 27). Global MBF was determined by manually delineating regions of interests in the anterior half of the mid-LV myocardium on the corresponding MBF maps.

Vascular Reactivity—Thoracic aortas were carefully removed and mounted on a multiwire myograph system (Danish Myo Technology) filled with physiological salt solution (PSS) under

normalized tension as previously described (28). Vessels were contracted by cumulative addition of increasing concentrations of phenylephrine in the organ bath. Contractions were expressed in millinewton/mm aortic ring length.

Cell Culture—H9C2 rat cardiac myoblasts were purchased from the ATCC and grown in Dulbecco's modified Eagle's medium supplemented with 10% fetal bovine serum and 1.5 g/liter of sodium bicarbonate.

Immunoprecipitation—Heart or H9C2 cells were washed with ice-cold PBS and lysed for 20 min on ice in lysis buffer supplemented with protease and phosphatase inhibitors as described (20). Protein was immunoprecipitated from lysates with anti-PMCA or anti-ShcA or nonimmune IgG and protein A/G Plus-agarose (Santa Cruz Biotechnology) as described previously (20). Precipitated proteins were separated by SDS-gel electrophoresis and immunoblotted with antibodies against PMCA, ShcA, and caveolin-1.

Isolation of Mouse Peritoneal Macrophages—Ctrl and smShcA$^-$ mice were injected intraperitoneally with 1 ml of 3% thioglycollate (Sigma) and peritoneal lavage was harvested 3 days later. These cells were tested for CD68 and galectin-3 expression by Western blot.

siRNA Transfections—H9C2 cells were plated and treated with siGENOME Smart Pool Shc1 siRNA according to the Dharmacon protocol. Cells were collected 3 days latter for protein analysis.

Confocal Microscopy—Cardiomyocytes isolated from control and smShcA$^-$ mice, and H9C2 cells were seeded on glass slides, fixed with paraformaldehyde, and incubated with anti-PMCA and anti-caveolin-1 or anti-IgG control primary antibodies and Alexa Fluor 488 and Alexa Fluor 546 secondary antibodies. Immunofluorescence-labeled cells were analyzed using a Leica TSC SPE confocal microscope with the ×63 oil immersion objective.

Protein and mRNA Expression Analysis—RNA was isolated using TRIzol reagent (Sigma) according to the manufacturer's instructions. 50 ng of RNA were converted to cDNA using the High-capacity cDNA Archive kit (Applied Biosystems, Foster City, CA). PCR amplification was performed using SYBR Green PCR master mixture (Applied Biosystems) according to the manufacturer's instructions. Primer sequences are available upon request. SDS-polyacrylamide gel electrophoresis and immunoblot analysis were performed according to standard procedures. Proteins were transferred onto nitrocellulose membranes and immunoblot analyses were carried out using antibodies directed against ShcA (Upstate), Cav-1 (Santa Cruz), Cav-3 (Santa Cruz), CD68 (Santa Cruz), dystrophin (Abcam, Cambridge, MA), galectin-3 (Abcam), paxillin (Santa Cruz), α7 (Santa Cruz), p44/42 Erk (Cell Signaling Technology), *p*-AKT (Cell Signaling Technology), P-mammalian target of rapamycin (Cell Signaling Technology), PMCA (Santa Cruz), or GAPDH (Sigma). Titin protein levels were quantified by vertical-agarose gel electrophoresis following the published protocol (29). Briefly, protein samples were prepared by homogenization of the LV in liquid N2 and lysis in 8 M urea, 50% (v/v) glycerol, DTT (80 mM final)/protease inhibitors (Roche Applied Science). Titin isoforms were separated by SDS-agarose gel electrophoresis followed by Coomassie Blue staining. AIDA software (Raytest) was used to quantify titin and myosin heavy chain (MHC) and GraphPad Prism (GraphPad Software, Inc.) for statistical analysis. For the titin domain phosphorylation assay, His_6-tagged Zis1 and Zis5 were amplified from mice heart cDNA by PCR using primer pairs: Zis1F (5′-TCCACTGCAGAATTGGTGGTTCAAG-3′), Zis1R (5′-GTAGAGCTTGTCATTGTCGTCTCTC-3′), Zis5F (5′-CATTGCAAGATGTCTGGATAT-3′), and Zis5R (5′-CAGTGACTGAGTTCCATCTTC-3′). The obtained fragments were subcloned into the pASK-IBA3 expression vector. His_6-tagged titin domains were purified and phosphorylation assays were done as previously described (30). Briefly, cell extracts from cardiac tissues of adult mice and embryos were added to phosphorylation assays buffer (25 mM Hepes, pH 7.2, 10 mM $MgCl_2$, 1 mM EGTA, 1 mM DTT, 0.2 mM ATP, and 1 mCi of [γ-^{33}P]ATP, 3,000 Ci/mM) at 37 °C for 10 min. The reactions were stopped by heating samples at 95 °C for 1 min and analyzed on 18% polyacrylamide gels. Gels were dried and autoradiographed with intensifying screens at −80 °C for 12 to 24 h.

Immunostaining Analysis—For immunostaining and histology experiments, hearts were cut longitudinally at the midventricular level, fixed with 4% paraformaldehyde in phosphate-buffered saline, embedded in paraffin, and cut in 5-μm slices as described (20). Sections were stained with eosin and hematoxylin for images of chamber cross-sections or with Sirius red to evaluate the degree of left ventricular interstitial fibrosis.

Statistical Analysis—Values are reported as mean ± S.E. of at least triplicate determinations. Statistical significance ($p < 0.05$) was determined using an unpaired Student's *t* test (GraphPad Prism, Abacus Concepts, Berkeley, CA).

RESULTS

Conditional ShcA Mutants Develop a Severe Cardiac Dysfunction and Die Prematurely—In offspring from matings between smShcA$^-$ (Sm22Cre$^+$, ShcA$^{flox/flox}$) and control mice (Sm22Cre$^-$, ShcA$^{flox/flox}$) the three ShcA isoforms were efficiently reduced in the heart during embryogenesis (E14.5, E18.5) and in the adults (Fig. 1*A*). Animals were born following the expected Mendelian ratios, but about 5% of conditional mutant mice died prematurely (Fig. 1*B*). Death was sudden suggesting an acute event, whereas no change was observed in body weight (26.2 ± 0.65 g in 3-month-old mutants, *versus* 27.6 ± 0.71 g in controls, not significant). Surviving smShcA$^-$ mice exhibited leg edema (Fig. 1*C*), a frequent sign of heart failure. In surviving smShcA$^-$ mice, hearts were enlarged with dilation of the left ventricle (Fig. 1*D*). Heart diameter and function in adults were followed by echocardiography. Compared with controls, left ventricle weight was increased in mutant mice (136 ± 13 mg in mutants, *versus* 102 ± 6 mg in controls, $p < 0.05$) at 3 months of age (Table 1). Left ventricle to body weight ratios of adult conditional mutants calculated from echocardiography were also increased relative to controls by 30% (5.2 ± 0.4 mg/g in mutants, *versus* 3.7 ± 0.1 mg/g in controls, $p < 0.01$), a further indication of cardiac hypertrophy (Table 1). The average left ventricular end-systolic (4.6 ± 0.4 mm in mutants, *versus* 2.9 ± 0.1 mm in controls, $p < 0.001$) and end-diastolic diameters (5.4 ± 0.3 mm in mutants, *versus* 4.4 ± 0.1 mm in controls, $p < 0.01$) were substantially increased in mutant mice

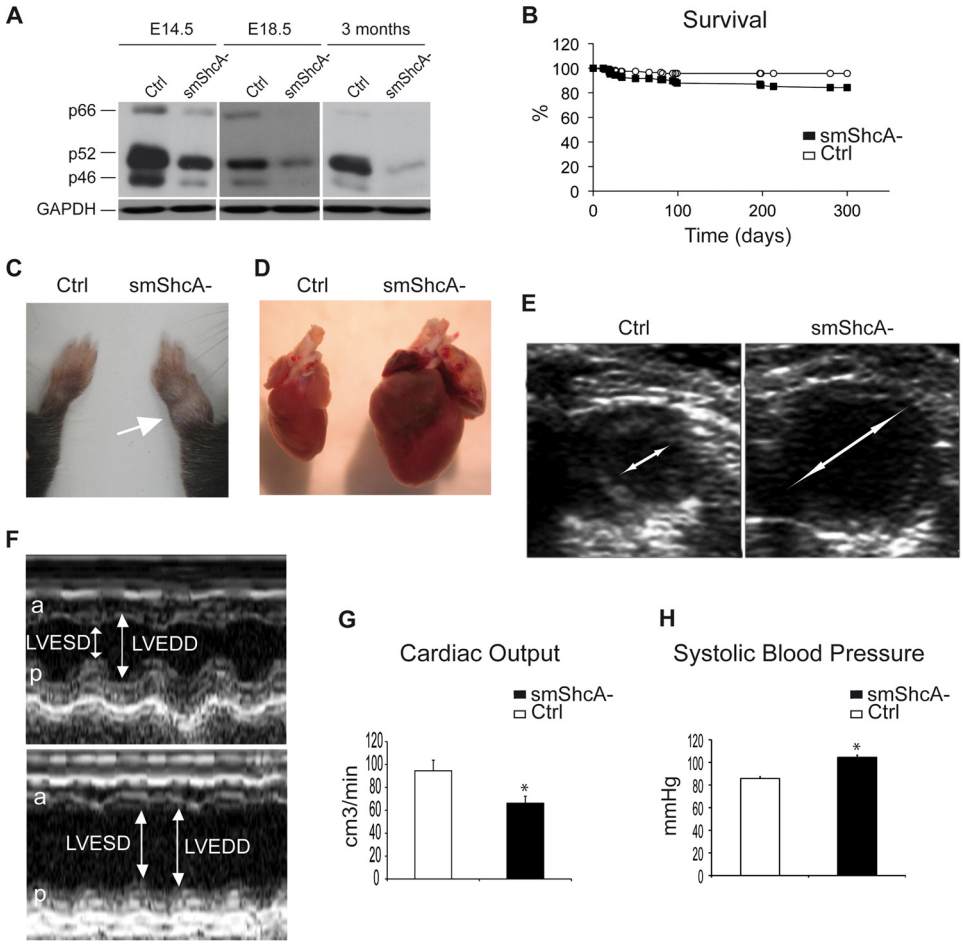

FIGURE 1. **Reduced survival and left ventricular dysfunction in smShcA$^-$ adult mice.** *A*, Western blot analysis of ShcA in embryonic hearts at E14.5, E18.5, and in hearts from 3-month-old smShcA$^-$ and control mice (*Ctrl*). *B*, Kaplan Meier curves showing reduced survival of smShcA$^-$ mice compared with control littermates (*Ctrl*) from birth (1 day) to 10 months old. *C*, representative image of leg edema (*arrow*) in 6-month-old smShcA$^-$ mice. *D*, gross anatomy of cardiac enlargement in 6-month-old mutant mice and littermate controls. *E*, echocardiographic cardiac output measurements in 3-month-old mutant and control mice. *F*, echocardiographic images (axial and M-mode) showing the anterior (*a*) and posterior (*p*) wall thickness as well as the increase in the LVEDD, and the LVESD in representative 3-month-old smShcA$^-$ mice (*bottom*) and littermate controls (*top*). *G*, quantification of cardiac output in 3-month-old mutant mice and littermate controls. *H*, increased systolic blood pressure in 3-month-old mutant mice (smShcA$^-$) compared with controls (*Ctrl*). For *panels G* and *H*, values are mean ± S.E. with *, $p < 0.05$ compared with littermate controls. $n \geq 10$ per group.

TABLE 1

Echocardiographic parameters

Echocardiography of smShcA$^-$ mice and controls.

	Controls ± S.E.	smShcA^{-a} ± S.E.	*p*
LV[b] weight (mg)	102 ± 6	136 ± 13	<0.05
LV weight/total weight (mg/g)	3.7 ± 0.1	5.2 ± 0.4	<0.01
LVEDD (mm)	4.4 ± 0.1	5.4 ± 0.3	<0.01
LVESD (mm)	2.9 ± 0.1	4.6 ± 0.4	<0.001
Fractional shortening (%)	35 ± 2	17 ± 2	<0.001
Ejection fraction (%)	71 ± 3	40 ± 4	<0.001
Heart rate (beats/min)	421 ± 7	428 ± 17	NS[c]
Aortic root diameter (mm)	0.15 ± 0.01	0.16 ± 0.01	NS

[a] smShcA$^-$, cardiovascular-specific ShcA knockout mice ($n > 6$ per group).
[b] LV, left ventricle.
[c] NS, not significant.

(Fig. 1, *E* and *F*, and Table 1). Fractional shortening (17 ± 2% in mutants, *versus* 35 ± 2% in controls, $p < 0.001$), a measure of cardiac output (Fig. 1*G*) and ejection fraction (40 ± 4% in mutants, *versus* 71 ± 3% in controls, $p < 0.001$) were all markedly impaired in smShcA$^-$ mice (Table 1). Echocardiography also revealed frequent arrhythmias and loss of contractility in large territories of smShcA$^-$ hearts (supplemental Videos S1 and S2). A moderate but significant increase in systolic blood pressure (Fig. 1*H*) with no change in heart rate (Table 1) was observed in adult smShcA$^-$ mice. Pulmonary hypertension, which is an additional sign of heart failure, was also observed in several mice during echocardiography through the observation of an enlarged right ventricle. Moreover, ECG examination showed a T-wave inversion caused by slowed ventricular repolarization in the mutant compared with controls, whereas *in vivo* noninvasive quantitative myocardial perfusion mapping using magnetic resonance images (MRI) showed normal coronary perfusion in mutant mice (Fig. 2*A*) with no change in myocardial blood flow (5.8 ± 0.4 ml/g/min in mutants, *versus* 6.5 ± 0.5 ml/g/min in controls, not significant). Defects are present before birth. With aging, cardiac function did not decline further. Fractional shortening (17.1 ± 2.2% at 3 months old, *versus* 16.0 ± 0.5% at 9 months old, not significant) and ejection fraction (41.5 ± 4.6% at 3 months old, *versus* 38.2 ± 0.8% at 9 months old, not significant) remained unchanged at 3 months compared with 9-month-old smShcA$^-$ mice.

Histological analysis of adult conditional mutant and control mice revealed enlarged ventricular chambers in smShcA$^-$ animals, abnormal tissue organization and morphology, and dis-

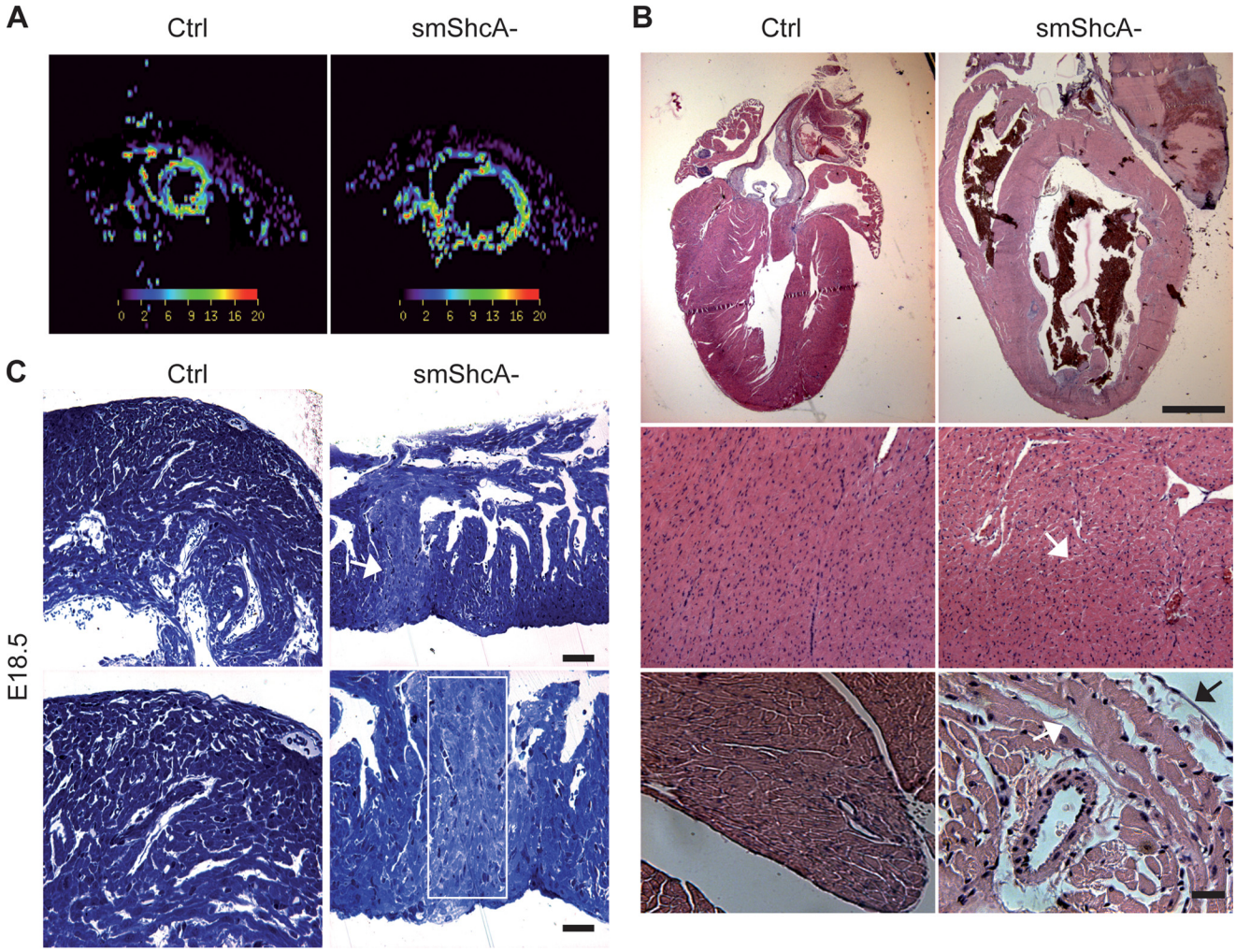

FIGURE 2. **Cardiac necrosis in the absence of ShcA.** *A*, color-coded cardiac perfusion (MBF) maps representative for each group of 3-month-old animals. *B*, H&E-stained sagittal (*top*) and axial (*bottom*) sections from 3-month-old smShcA$^-$ mice hearts and littermate controls. The *white arrow* shows disruption of the tissue. *Scale bars*, top panels = 3 mm; bottom panels = 200 μm. *C*, toluidine blue staining shows necrotic regions in the heart from smShcA$^-$ mice and controls at E18.5 (*white arrow* and *white square*). *Scale bars*, top panels = 500 μm; bottom panels = 200 μm.

ruption of myofibrils (Fig. 2*B*). Histological evidence of myocardial infarction, such as necrotic areas, were observed as early as embryonic day E18.5 (Fig. 2*C*). Masson's trichrome and Sirius red staining did not reveal any increase in myocardial interstitial fibrosis in smShcA$^-$ mice compared with controls (data not shown).

Effects of ShcA Deficiency Are Largely Compensated in the Vasculature—The Sm22 protein is expressed in both vascular and visceral smooth muscle cells and more recently it was detected in myeloid cells (31). We examined the expression of ShcA in visceral smooth muscle cell-containing tissues such as intestine, bladder, lung, muscle, spleen, and macrophages (31), and found no difference in smShcA$^-$ mice compared with controls (Fig. 3*A*). Thus, it is unlikely that these tissues contributed to the observed phenotype. Because in vascular smooth muscle cells ShcA levels are strongly decreased (Fig. 3*A*), we evaluated the vascular contribution to the observed cardiac phenotype. Histological analysis of H/E-stained aorta showed no significant difference in tissue organization and morphology (Fig. 3*B*, *left panel*). Also no difference in tissue organization was observed in electron microscopy (Fig. 3*B*, *right panel*). Similarly, there was no difference in aortic root diameter in smShcA$^-$ compared with control mice (Table 1). We further tested whether the moderate increase in blood pressure could be explained by an altered vascular reactivity. In aortas from smShcA$^-$ *versus* control animals there was no significant difference in the vasoconstrictive response upon phenylephrine treatment (Fig. 3*C*). However, this does not rule out a potential contribution of altered microvascular reactivity to the hypertensive state. Vascular smooth muscle cells are known to play a role in the development of atherosclerotic lesions, and ShcA is able to bind to the cytoplasmic tail of LRP1, a transmembrane receptor known to protect against atherosclerosis when expressed in vascular smooth muscle cells (20). As atherosclerosis is a risk factor frequently associated with cardiovascular disease in humans, we assessed if atheroprone conditions would worsen the cardiac phenotype of smShcA$^-$ mice. Accordingly, we bred the mice on a LDL receptor deficiency background to increase their susceptibility for atherosclerosis, fed them an atherogenic diet, and analyzed the atherosclerotic phenotype. In contrast to LRP1-deficient mice, Sm22cre-medi-

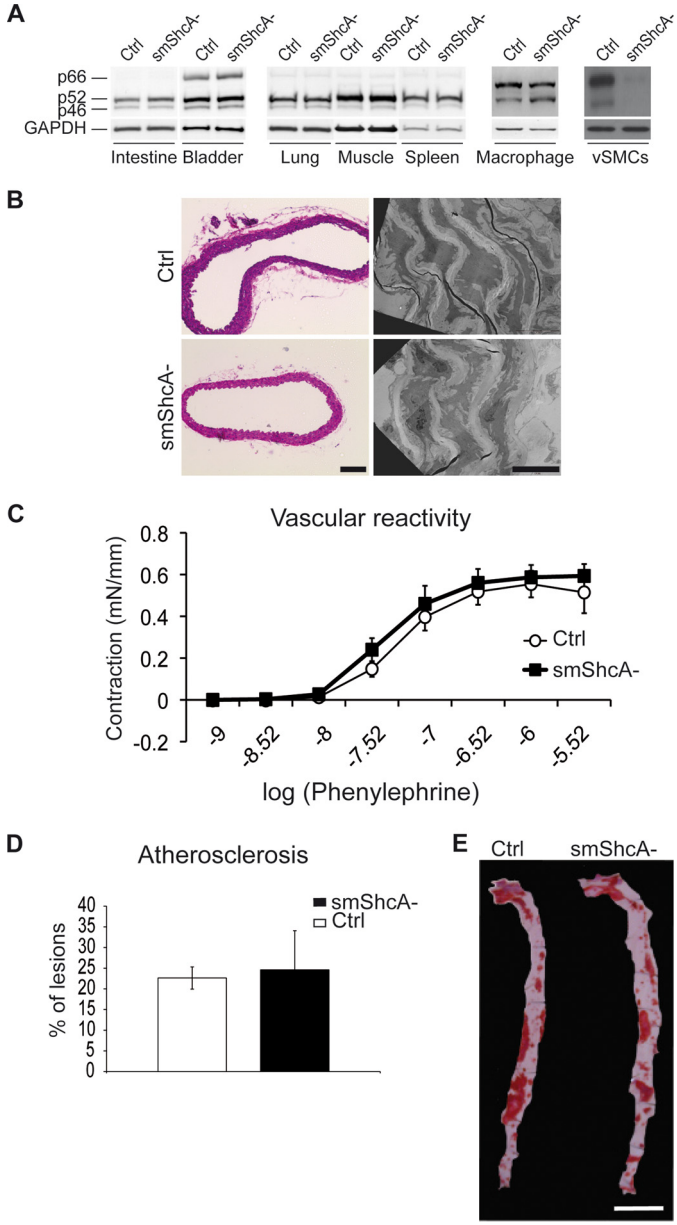

FIGURE 3. **Absence of vascular phenotype when ShcA is deleted in vascular smooth muscle cells.** *A*, Western blot analysis of ShcA in the indicated tissues from 3-month-old smShcA^{-} and control mice (*Ctrl*). *B*, H&E staining and electron microscopy analysis of aortas from smShcA^{-} mice and controls. *Scale bars* = 200 mm (*left panels*) and 10 μm (*right panels*). *C*, vascular reactivity upon phenylephrine treatment ($n = 5$ per group, 3-month-old mice). *D*, quantitative analysis of atherosclerotic lesion size in aortas from cholesterol-fed mice ($n = 6$ per group). *E*, opened and Sudan IV-stained aortas from cholesterol-fed mice that express or lack ShcA in vascular smooth muscle cells. *Scale bars* = 1 cm. Values are mean ± S.E.

ated ablation of ShcA did not lead to an increase in atherosclerotic lesions, even when mice were bred on a background of LDLr deficiency and fed an atherogenic diet, as demonstrated by size measurements of lesions (Fig. 3*D*), and *en face* analysis of the aortic lesion area (Fig. 3*E*). Furthermore, under these atheroprone conditions, echocardiographic parameters did not worsen (data not shown). Thus, we did not find any obvious abnormalities in the vascular system of ShcA mutant mice. This suggests that there is no vascular contribution to the cardiac phenotype in ShcA-deficient mice.

Abnormal ErbB3 Signaling in the Hearts of Conditional Mutant Mice—We next evaluated the molecular basis of the dilated cardiomyopathy phenotype in the absence of ShcA. Because the heart has achieved its definitive configuration by E15.5 (except for the atrioventricular valve leaflets and coronary artery) (32), we analyzed embryos between E14.5 and E18.5. Although ShcA has been reported to be critical for MAPK activation or the switch from AKT/mammalian target of rapamycin toward Erk activation (33), there were no significant changes in phospho-Erk, phospho-AKT, or phospho-mammalian target of rapamycin indicative of Erk or AKT activation, in heart lysates from E14.5, E18.5, or 3-month-old mutant mice compared with controls (data not shown). However, we observed marked disruption of myofibrillar architecture and mitochondrial hyperplasia, which were already present at E14.5 in mutant cardiomyocytes, as revealed by electron microscopy (Fig. 4*A*). At E18.5, we found myofibrillar disarray (Fig. 4*A*). This includes severe changes in the Z-disk and M-band of the sarcomere. Z-disks link myofilaments to membrane systems, specifically to the T-tubules (34, 35), and transmit biomechanical stress through associated signaling proteins (36). In smShcA mutants at E18.5 as sarcomeres matured, we observed Z-disk thickening (Fig. 4, *A* and *B*), as well as loss of defined M-band structures (Fig. 4*A*). Morphology was abnormal, with bubbling and misalignment of T-tubules with Z-disk components (Fig. 4*A*). To link ShcA to Z-disk- and T-tubules-associated abnormalities, we studied the ErbB receptor tyrosine kinase pathway, which is important for T-tubule integrity and protects against dilated cardiomyopathy (3, 4). Furthermore, the PTB domain of ShcA interacts with tyrosine kinase receptors including ErbB (5). We found that protein levels of the ErbB3 receptor were significantly decreased at E14.5 in mutants compared with controls (0.55 ± 0.04 in mutants, *versus* 0.75 ± 0.04 in controls, $p < 0.05$) (Fig. 4*C*). No significant change was found at E18.5 (0.59 ± 0.04 in mutants, *versus* 0.62 ± 0.02 in controls, not significant) (Fig. 4*C*). ErbB3 receptor protein expression levels were almost undetectable in adult mice (data not shown), however, ErbB3 receptor mRNA levels were decreased in adult mutants compared with controls (Fig. 4*D*). There was no difference in the relative mRNA levels of ErbB2 (0.98 ± 0.52 in mutants, *versus* 1 in controls, not significant) and ErbB4 receptors (1.04 ± 0.25 in mutants, *versus* 1 in controls, not significant) compared with controls. In agreement with an altered ErbB3 signaling in the absence of ShcA, we found in mutants at E18.5, a decrease in protein levels of both p26 (0.58 ± 0.04 in mutants, *versus* 0.75 ± 0.04 in controls, $p < 0.01$) and p30 (0.45 ± 0.04 in mutants, *versus* 0.62 ± 0.02 in controls, $p < 0.01$) active isoforms of Neuregulin-1 (Nrg-1), the ligand of the ErbB receptors (37). The p45 isoform remained unchanged (0.11 ± 0.01 in mutants, *versus* 0.16 ± 0.02 in controls, not significant). At E14.5, the protein levels of p26 (0.87 ± 0.13 in mutants, *versus* 0.83 ± 0.24 in controls, not significant), p30 (0.41 ± 0.08 in mutants, *versus* 0.53 ± 0.11 in controls, not significant), and p45 isoforms (0.11 ± 0.01 in mutants, *versus* 0.12 ± 0.01 in controls, not significant) remained unchanged. Thus in the absence of ShcA, ErbB3 dysregulation precedes abnormal expression of the p26 and p30 isoforms of Nrg-1. Upon binding of Nrg-1, ErbB receptors generate signals inside

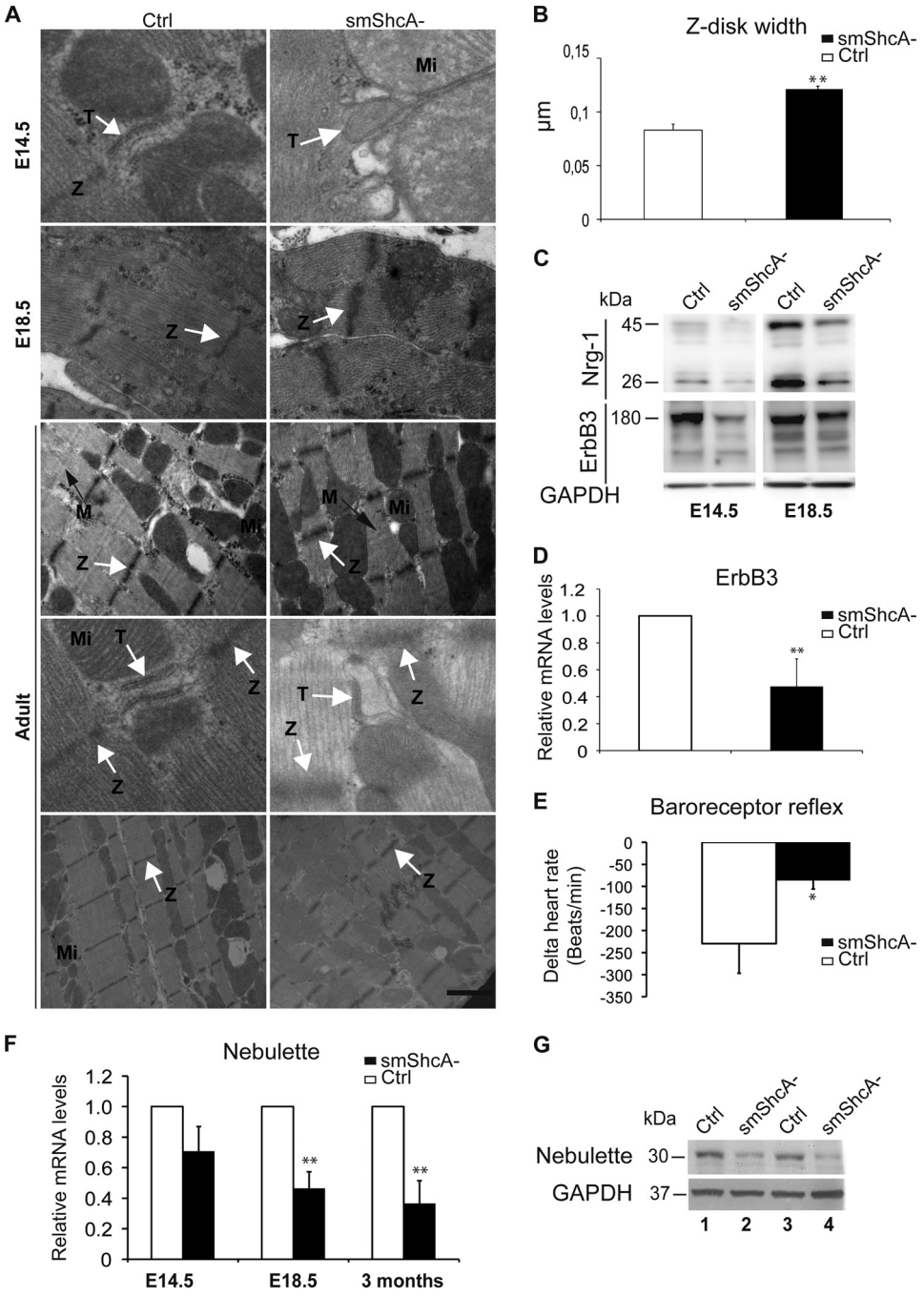

FIGURE 4. **Abnormal thin filament·Z-disk complex assembly in the absence of cardiac ShcA.** *A*, abnormal myofibrillar ultrastructure as determined by electron microscopy in conditional mutant (smShcA$^-$) and control (*Ctrl*) mice at E14.5, E18.5, and 3-month-old mice. Note the increase of the thickening of the Z-disks (*Z*) (E18.5 and adults, *top panels*, *white arrows*) and undefined M-band (M) structures (E18.5, adults, *dark arrows*) at embryonic stages. Mitochondrial (*Mi*) swelling (adult, *bottom panels*) and abnormal T-tubules (*T*) (E14.5 and adult, *middle panels*, *white arrows*), which are no longer aligned with Z-disks and of abnormal morphology (bubbling, E14.5) are present. *Scale bars*: E14.5 = 500 nm; E18.5 = 1 μm; adults, top = 1 μm; middle = 500 nm; bottom = 2 μm. *B*, Z-disk width in the heart from mutant (smShcA$^-$) and (*Ctrl*) control embryos at E18.5 ($n = 4$ per group). *C*, protein levels of the ErbB3 receptor and its ligand Nrg-1 at E14.5 and E18.5, in mutant (smShcA$^-$) and (*Ctrl*) control hearts ($n = 4$ per group). *D*, mRNA levels of the ErbB3 receptor in 3-month-old mice ($n = 6$ per group). *E*, measurements of the heart rate upon phenylephrin treatment in 3-month-old mutants (smShcA$^-$) and controls. Measurements were done in a minimum of 6 mice per group. *F*, time course of the mRNA levels of nebulette between E14.5 and 3 months of age, in mutants (smShcA$^-$) and controls ($n = 4$ per group). *G*, protein levels of nebulette in 3-month-old mice. Values are mean ± S.E. with *, $p < 0.05$ and **, $p < 0.01$ compared with littermate controls.

cells that diminish the inotropic response to adrenergic stimulation, thereby mimicking an anti-adrenergic effect of muscarinic cholinergic receptor signaling (38). Consistent with a down-regulation of ErbB3 signaling, we found an altered baroreceptor reflex-induced decrease in the heart rate upon phenylephrine treatment in the mutants (Fig. 4*E*). Taken together, these data argue for a role of the ShcA-mediated ErbB3 signaling in sarcomere function and integrity in the heart.

The cardiac homologue of nebulin, nebulette, is a sarcomeric Z-disk protein involved in force generation via its interaction with the actin and tropomyosin·troponin complex and plays a critical role in the formation of the thin filament·Z-line com-

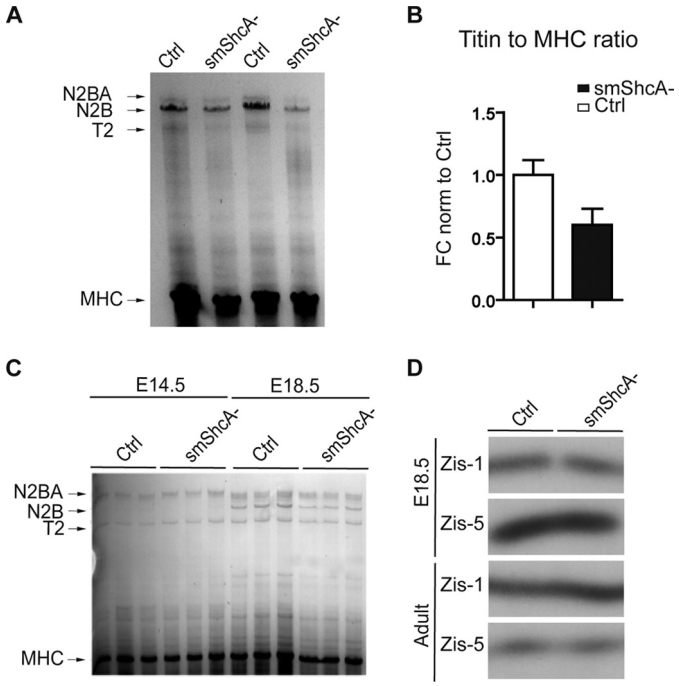

FIGURE 5. **Titin signaling in the absence of cardiac ShcA.** *A*, SDS-agarose gel electrophoresis and Coomassie Blue staining of titin in hearts from 3-month-old mutants (smShcA$^-$) and controls. *B*, quantification of SDS-agarose gel electrophoresis. *C*, SDS-agarose gel electrophoresis and Coomassie Blue staining of titin in the heart from mutants (smShcA$^-$) and control embryos. *D*, ^{32}P-phosphorylation of the recombinant titin Z-disk fragments Zis-1 and Zis-5 upon treatments with heart lysates from E18.5 and 3-month-old mutant and control mice. Values are mean ± S.E.

plex early during myofibrillogenesis (39). Mutations of nebulette lead to increased Z-disk thickening, enlarged T-tubules (40), dilated cardiomyopathy, and severe heart failure in mice and humans (41). Because these events recapitulated most of the phenotype observed in smShcA$^-$ mice, we tested nebulette signaling in the absence of cardiac ShcA. We found that mRNA levels of nebulette were down-regulated in E18.5 embryos, as well as in adult hearts from smShcA$^-$ mice compared with controls (Fig. 4*F*). Similarly, protein levels of nebulette were down-regulated in adult hearts from smShcA$^-$ mice compared with controls (Fig. 4*G*). Together, these data indicate that ShcA mutation selectively affects nebulette expression in the Z-disk, an event that can cause abnormal Z-disk assembly (40), and might contribute to altered muscle force generation via the interaction of nebulette with actin and the cardiac tropomyosin·troponin complex.

ShcA Mutation Differentially Affects Expression of Sarcomeric Proteins—Titin is a giant protein (over 3 MDa) that extends from the Z-disk to the M-band of the sarcomere (42) and has been associated with human cardiac disease (43–46). In the Z-disk, the sequence insertions Zis-1 and Zis-5 contain *X*SP*X*R motif repeats that have been shown to be phosphorylated *in vitro* by ERK1/2, an event that might require ShcA (30, 48). We first measured the protein level of titin and found no significant difference in embryonic or adult mutant mice (Fig. 5, *A–C*), compared with controls. Using immunoprecipitation experiments, we then measured phosphorylation of the recombinant Zis-1 and Zis-5 motifs of titin in heart lysates. There was no difference in the phosphorylation of these motifs between mutants and controls (Fig. 5*D*). Thus, it is unlikely that alterations of titin expression or posttranslational Z-disk modification account for the observed cardiac phenotype in smShcA$^-$ mice.

ShcA Mutation Selectively Affects the Dystrophin Complex Signaling Pathway—Because ShcA interacts with Cav-1, we measured the expression of Cav-1 and Cav-3 and found a higher protein level of Cav-1 (Fig. 6, *A, B*, and *D*) in the heart of adult smShcA$^-$ mice compared with controls, whereas Cav-3 protein expression was unaffected (Fig. 6, *B* and *D*). Consistently, electron microscopy analysis showed more caveolae formation in adult hearts from smShcA$^-$ mice compared with controls (Fig. 6*C*). Cav-1 also interacts with β-dystroglycan and the DGC complex (49). Thus, we determined whether dystrophin signaling is altered in smShcA$^-$ mice. We found a strong redistribution of dystrophin labeling by immunohistochemistry analysis (Fig. 6*A*) and a substantial increase in dystrophin protein expression in the heart from smShcA$^-$ adult mice (Fig. 6, *B* and *D*) and embryos at E14.5 (Fig. 6*E*) compared with controls. Furthermore, we found that the costameric protein PMCA co-immunoprecipitated with ShcA and Cav-1 in heart lysates from control mice, whereas in the heart from smShcA$^-$ mice, PMCA is absent from the complex (Fig. 7*A*). The same results were observed in H9C2 rat cardiac myoblasts treated with ShcA siRNA or control (Fig. 7*B*). There was no difference in PMCA mRNA levels between mutant and control hearts (PMCA-1, 0.85 ± 0.07 *versus* 1; PMCA-2, 0.95 ± 0.02 *versus* 1; PMCA-4, 1.11 ± 0.13 *versus* 1, not significant). Similarly, immunofluorescent staining of Cav-1 and PMCA in isolated cardiomyocytes from smShcA$^-$ and control mice (Fig. 7*C*) or in H9C2 rat cardiac myoblasts treated with ShcA siRNA or controls (Fig. 7*D*) showed co-localization of both proteins when ShcA is expressed. We did not find any differences in the protein expression of the α7β1 integrin (Fig. 6, *B* and *D*) and its downstream target paxilin (Fig. 6, *B* and *D*), which also signals in costameres, suggesting that only the DGC is affected by the absence of ShcA. Together, these data demonstrate that ShcA is localized at costameres. They reveal an interaction between ShcA, PMCA, and Cav-1, and indicate a role of ShcA in the spatial organization of the costamere/Z-disk network, and cardiomyocyte contraction.

DISCUSSION

In this study, we used a conditional knock-out of ShcA to understand its function early during heart development and in the progression of cardiovascular disease. We used Cre-*lox*P-mediated recombination to introduce the ShcA deletion in cardiomyocytes and found that the conditional mutant mice develop a severe dilated cardiomyopathy, which is associated with signs of myocardial infarction, such as T-wave inversions and large necrotic areas, and occurrence of sudden death. The numerous abnormalities seen in the sarcolemma demonstrate for the first time that ShcA is required for sarcomere structure and integrity during heart development. In particular, ShcA is needed for a normal morphology of Z-disks and T-tubules. To delete ShcA in the cardiovascular system early during development we used the Cre transgene under the control of the sm22 promoter expressed from E8.5 (19). In mice, a single beating

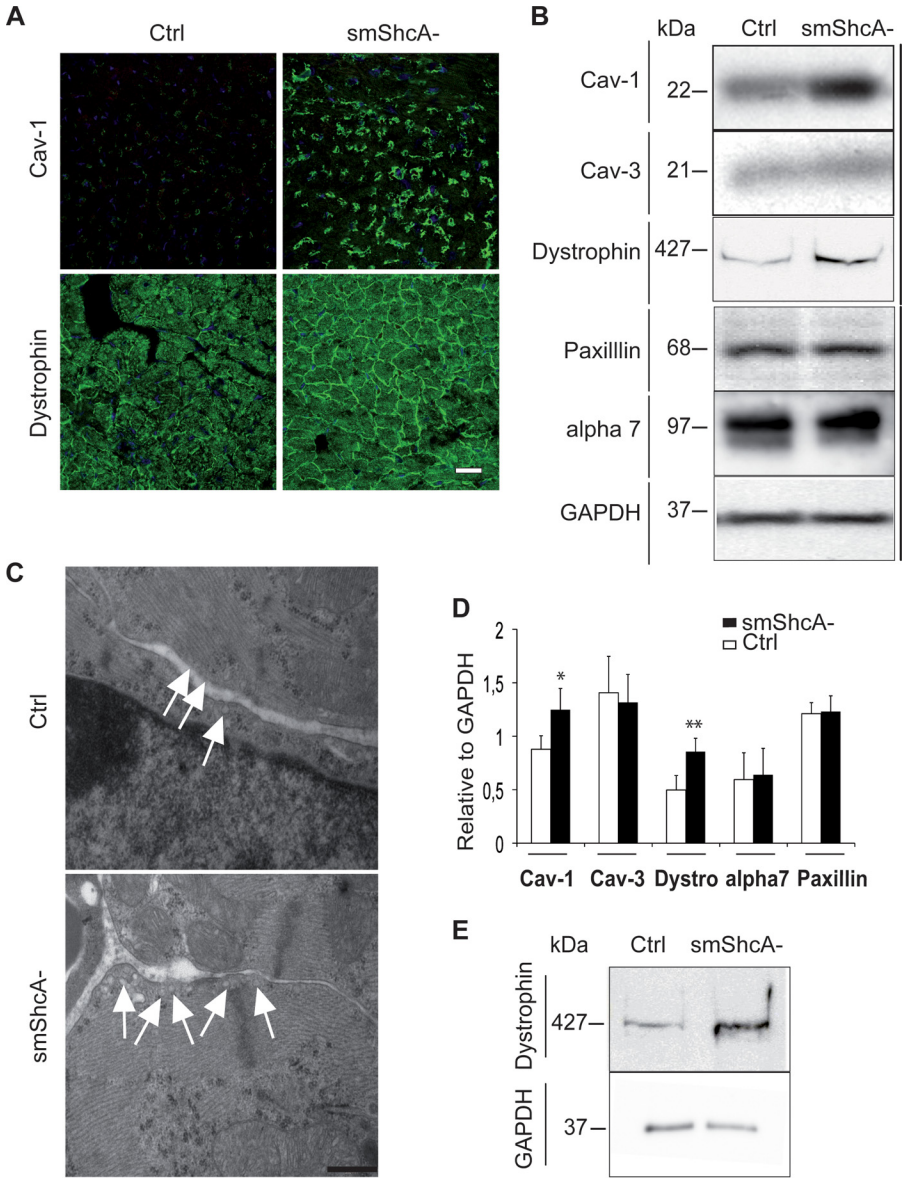

FIGURE 6. **Abnormal dystrophin signaling in the absence of cardiac ShcA.** *A*, immunostaining of Caveolin-1 and dystrophin in 3-month-old conditional mutant (smShcA$^-$) and control (*Ctrl*) hearts. Note the increase in the thickening of the dystrophin staining in the sarcolemma. *Scale bars* = 100 μm. *B*, Western blot of the indicated proteins in heart lysates from 3-month-old and, *E*, embryo (E14.5) conditional mutants (smShcA$^-$) and controls. *C*, electron microscopic analysis of caveolae in 3-month-old conditional mutant (smShcA$^-$) and control hearts. *Scale bars* = 1 μm. *D*, Western blot densitometric scanning of the relative protein expressions of caveolin-1 (*Cav-1*), caveolin-3 (*Cav-3*), dystrophin (*Dystro*), α7 integrin (*alpha7*), and paxillin in the heart from 3-month-old mutants (smShcA$^-$) and (*Ctrl*) controls ($n = 4$ per group). *E*, Western blot of dystrophin in embryo (E14.5) conditional mutants and controls. Values are mean ± S.E. with *, $p < 0.05$ and **, $p < 0.01$.

heart tube is formed by E8.0. At first, the contractions are irregular, but by E9.0 a regular heartbeat is established (50). In the smShcA$^-$ mice at E14.5, when atrial septation is not complete and the heart has not yet achieved its definitive prenatal configuration (32), ShcA was already efficiently deleted (Fig. 1*A*). Previous reports suggested that the elimination of ShcA after birth in cardiomyocytes using a Cre-*lox*P strategy with myosin light chain-driven Cre recombinase (ShcA CKO mice), led to a moderate cardiac phenotype (10). There was no evidence of myofibrillar abnormalities, aberrant intercalated disks structure, or mitochondrial abnormalities in these mice (10). This can be attributed to the late expression of the myosin light chain transgene, starting at 2 weeks of age with efficient reduction of ShcA expression at 12 weeks of age (10). Thus, the striking difference between the onset of cardiomyopathy in smShcA$^-$ mice *versus* ShcA CKO mice (10) is most likely due to the earlier reduction of ShcA in the smShcA$^-$ mice. Alternatively, differences in the genetic background of the two lines of mice may have a role, which might imply the existence of modifying loci important for normal heart function in the absence of ShcA signaling. Because the deletion occurs both in the heart and in the vascular wall, we could not exclude a contribution of the vascular system to the cardiac phenotype. However, we have been unable to detect any vascular modification in the absence of ShcA that may explain or contribute to the phenotype in the heart. This also demonstrates that the expression of ShcA in vascular smooth muscle cells is not crucial for the development of the vascular system. The only modification observed was a

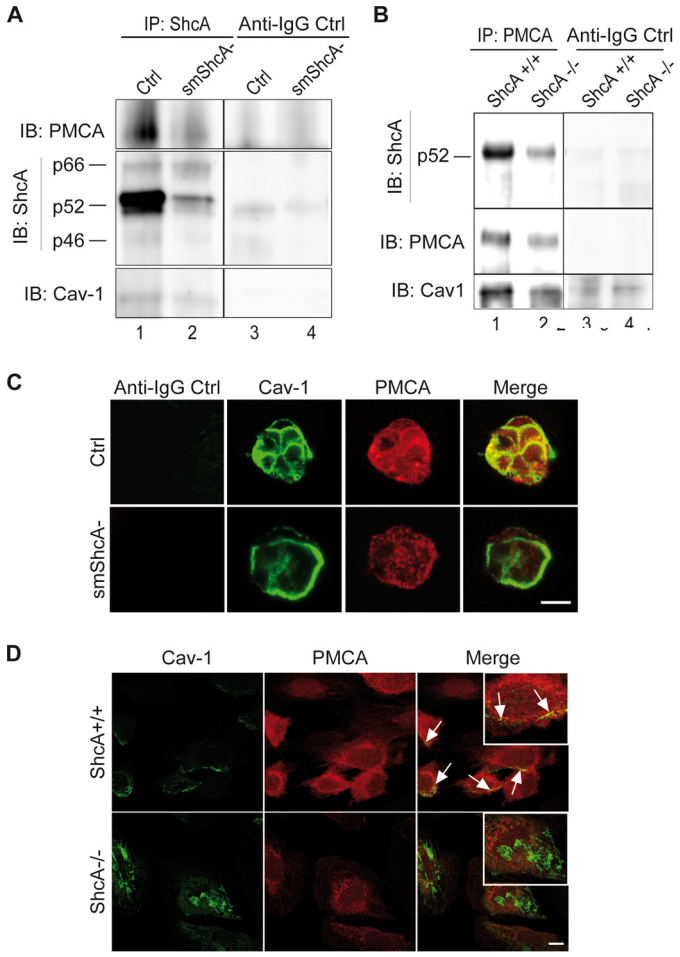

FIGURE 7. **ShcA and PMCA are associated in the heart dystrophin·glycoprotein complex.** *A*, co-immunoprecipitation between ShcA, PMCA, and Cav-1 in heart lysates from smShcA$^-$ and control mice. *B*, co-immunoprecipitation between PMCA, P52 ShcA, and Cav-1 in H9C2 rat cardiac myoblasts treated with ShcA siRNA (ShcA$^{-/-}$) or controls (ShcA$^{+/+}$). *C*, immunofluorescent staining of Cav-1 and PMCA in isolated cardiomyocytes from 3-month-old smShcA$^-$ and control mice. *D*, immunostaining of Cav-1 and PMCA in H9C2 rat cardiac myoblasts treated with ShcA siRNA (ShcA$^{-/-}$) or controls (ShcA$^{+/+}$). *Scale bars* = 10 μm.

moderate increase in systolic blood pressure. However, the histological and electron microscopy data obtained at E14.5 and E18.5 strongly argues against pressure overload from systemic hypertension as a major cause of the initial development of heart failure. Hypertension development on an already dysfunctional heart may, however, accelerate heart failure resulting in premature death.

Nrg-1/ErbB signaling, which is enriched in T-tubules, is indispensable in cardiac development (3, 4). Upon binding to Nrg-1, ErbB regulates the expression of several sarcomeric proteins, as well as cell-cell and cell-matrix interactions (37). Both, the heart-specific knock-out of ErbB2 and its co-receptor ErbB4 results in dilated cardiomyopathy (3, 4, 51). Furthermore, the Nrg-1/ErbB pathway has been described as a potential novel therapeutic target for heart failure (52, 53). Despite the fact that ShcA interacts with ErbB receptors (54), we did not find any changes in the expression of ErbB2 or ErbB4. Furthermore, in the case of the ErbB2 cardiomyocyte conditional mutants, a normal myofibrillar ultrastructure was observed by electron microscopy (3, 4), which was not the case in smShcA$^-$ mice. In contrast, we found that protein and mRNA levels of the ErbB3 receptor, which also localize to the Z-disks (55), are down-regulated in the adult heart. ErbB3 is expressed in prenatal cardiac myocytes and vascular endothelial cells (56) and has been reported in adult mouse cardiac myocytes (55). However, unlike ErbB2/4 receptors, which have now gained large recognition, the role of the ErbB3 receptor in maintaining heart function is not well known. Mice with a null mutation for ErbB3 die in uterus at day E13.5 (57). Here we found that in the absence of ShcA during heart development, ErbB3 protein expression is severely altered at E14.5 (Fig. 4*C*) and precedes a decrease in Nrg-1 protein expression at E18.5 (Fig. 4*C*). These data, along with the abnormal baroreceptor reflex response observed in the absence of ShcA, and which have been associated with ErbB signaling, strongly suggests that the ErbB3 receptor is functionally deficient when ShcA is deleted before E14.5, and that integrity of the ErbB3/ShcA pathway during embryogenesis is required to maintain cardiac function in the adult.

α7/β1-Integrins are transmembrane proteins located at the periphery of costameres that link the contractile apparatus to the extracellular matrix, thereby playing an essential role in sensing mechanical stress and in mechanotransduction (58). The Z-disk protein complex that relay α7/β1-integrin signals is composed of proteins such as talin, paxillin, and vinculin. Talin is a cytoskeletal protein that directly interacts with α7/β1-integrins through its F1 and F3 domains (59). It was previously demonstrated that ShcA binds to integrins (5, 6). However, we did not find any modification in the protein levels of α7/β1-integrins in the absence of ShcA. Neither had we found any modification in the protein expression of the talin downstream signaling protein, paxillin in smShcA$^-$ mice compared with controls. Thus, in the absence of ShcA, the α7/β1-integrin pathway is not altered and ShcA does not cooperate with the integrin/talin outside-in signal. In costameres, Cav-1 and -3 are important components of the DGC. Cav-1-deficient mice have demonstrated cardiac hypertrophy because of hyperactivation of one of the ShcA target, Erk1/2 (47, 60). Because Cav-1 physically and functionally interacts with ShcA in caveolae (11), we evaluated its expression in smShcA$^-$ mice. The substantial increase of Cav-1 protein levels in the smShcA$^-$ mice heart associated with an increase in the formation of caveolae demonstrated that signaling through Cav-1 is altered in these mice. In agreement, we found a profound redistribution of dystrophin labeling by immunofluorescence analysis associated with an increase in the dystrophin protein levels in smShcA$^-$ mice hearts.

In the DGC, dystrophin binds to α-syntrophin, which in turns interacts with PMCA (14). Furthermore, a functional interaction between ShcA and PMCA was previously suggested (17). Thus, PMCA could directly or indirectly interact with ShcA and associate with Cav-1 and α-syntrophin in the DGC. Our data suggest that PMCA organizes such a macromolecular complex in costameres, where ShcA by binding to both Cav-1 and PMCA links the contractile apparatus to the extracellular matrix and thus plays a central role in cardiac function.

In conclusion, we demonstrate for the first time that ShcA was localized to the DGC in the heart suggesting a role of ShcA in protecting costameres/Z-disk axis structure and integrity,

and highlight ShcA as a new molecule for appropriate heart formation during development.

Acknowledgments—We are grateful to Manuel Mark, Jean Marie Garnier, and Jean Marc Bornert (IGBMC, University of Strasbourg) for technical advice and expertise, and Daniel Metzger (IGBMC, University of Strasbourg) for critical reading of the manuscript.

REFERENCES

1. Watkins, H., Ashrafian, H., and Redwood, C. (2011) Inherited cardiomyopathies. *N. Engl. J. Med.* **364,** 1643–1656
2. Liew, C. C., and Dzau, V. J. (2004) Molecular genetics and genomics of heart failure. *Nat. Rev. Genet.* **5,** 811–825
3. Crone, S. A., Zhao, Y. Y., Fan, L., Gu, Y., Minamisawa, S., Liu, Y., Peterson, K. L., Chen, J., Kahn, R., Condorelli, G., Ross, J., Jr., Chien, K. R., and Lee, K. F. (2002) ErbB2 is essential in the prevention of dilated cardiomyopathy. *Nat. Med.* **8,** 459–465
4. Ozcelik, C., Erdmann, B., Pilz, B., Wettschureck, N., Britsch, S., Hübner, N., Chien, K. R., Birchmeier, C., and Garratt, A. N. (2002) Conditional mutation of the ErbB2 (HER2) receptor in cardiomyocytes leads to dilated cardiomyopathy. *Proc. Natl. Acad. Sci. U.S.A.* **99,** 8880–8885
5. Ravichandran, K. S. (2001) Signaling via Shc family adapter proteins. *Oncogene* **20,** 6322–6330
6. Wills, M. K., and Jones, N. (2012) Teaching an old dogma new tricks: twenty years of Shc adaptor signalling. *Biochem. J.* **447,** 1–16
7. van der Geer, P., Wiley, S., Gish, G. D., and Pawson, T. (1996) The Shc adaptor protein is highly phosphorylated at conserved, twin tyrosine residues (Y239/240) that mediate protein-protein interactions. *Curr. Biol.* **6,** 1435–1444
8. Yajnik, V., Blaikie, P., and Margolis, B. (1998) Cloning and mutational analysis of the Shc-phosphotyrosine interaction/phosphotyrosine-binding domain. *Methods Mol. Biol.* **84,** 223–235
9. Lai, K. M., and Pawson, T. (2000) The ShcA phosphotyrosine docking protein sensitizes cardiovascular signaling in the mouse embryo. *Genes Dev.* **14,** 1132–1145
10. Vanderlaan, R. D., Hardy, W. R., Kabir, M. G., Pasculescu, A., Jones, N., deTombe, P. P., Backx, P. H., and Pawson, T. (2011) The ShcA phosphotyrosine docking protein uses distinct mechanisms to regulate myocyte and global heart function. *Circ. Res.* **108,** 184–193
11. Wary, K. K., Mariotti, A., Zurzolo, C., and Giancotti, F. G. (1998) A requirement for caveolin-1 and associated kinase Fyn in integrin signaling and anchorage-dependent cell growth. *Cell* **94,** 625–634
12. Balijepalli, R. C., and Kamp, T. J. (2008) Caveolae, ion channels and cardiac arrhythmias. *Prog. Biophys. Mol. Biol.* **98,** 149–160
13. Wu, X., Chang, B., Blair, N. S., Sargent, M., York, A. J., Robbins, J., Shull, G. E., and Molkentin, J. D. (2009) Plasma membrane Ca^{2+}-ATPase isoform 4 antagonizes cardiac hypertrophy in association with calcineurin inhibition in rodents. *J. Clin. Investig.* **119,** 976–985
14. Williams, J. C., Armesilla, A. L., Mohamed, T. M., Hagarty, C. L., McIntyre, F. H., Schomburg, S., Zaki, A. O., Oceandy, D., Cartwright, E. J., Buch, M. H., Emerson, M., and Neyses, L. (2006) The sarcolemmal calcium pump, α-1 syntrophin, and neuronal nitric-oxide synthase are parts of a macromolecular protein complex. *J. Biol. Chem.* **281,** 23341–23348
15. Pellegrini, M., Finetti, F., Petronilli, V., Ulivieri, C., Giusti, F., Lupetti, P., Giorgio, M., Pelicci, P. G., Bernardi, P., and Baldari, C. T. (2007) p66SHC promotes T cell apoptosis by inducing mitochondrial dysfunction and impaired Ca^{2+} homeostasis. *Cell Death Differ.* **14,** 338–347
16. Goellner, G. M., DeMarco, S. J., and Strehler, E. E. (2003) Characterization of PISP, a novel single-PDZ protein that binds to all plasma membrane Ca^{2+}-ATPase b-splice variants. *Ann. N.Y. Acad. Sci.* **986,** 461–471
17. Armesilla, A. L., Williams, J. C., Buch, M. H., Pickard, A., Emerson, M., Cartwright, E. J., Oceandy, D., Vos, M. D., Gillies, S., Clark, G. J., and Neyses, L. (2004) Novel functional interaction between the plasma membrane Ca^{2+} pump 4b and the proapoptotic tumor suppressor Ras-associated factor 1 (RASSF1). *J. Biol. Chem.* **279,** 31318–31328
18. Li, L., Miano, J. M., Cserjesi, P., and Olson, E. N. (1996) SM22αalpha, a marker of adult smooth muscle, is expressed in multiple myogenic lineages during embryogenesis. *Circ. Res.* **78,** 188–195
19. Malhowski, A. J., Hira, H., Bashiruddin, S., Warburton, R., Goto, J., Robert, B., Kwiatkowski, D. J., and Finlay, G. A. (2011) Smooth muscle protein-22-mediated deletion of Tsc1 results in cardiac hypertrophy that is mTORC1-mediated and reversed by rapamycin. *Hum. Mol. Genet.* **20,** 1290–1305
20. Boucher, P., Gotthardt, M., Li, W. P., Anderson, R. G., and Herz, J. (2003) LRP: role in vascular wall integrity and protection from atherosclerosis. *Science* **300,** 329–332
21. Seznec, H., Simon, D., Monassier, L., Criqui-Filipe, P., Gansmuller, A., Rustin, P., Koenig, M., and Puccio, H. (2004) Idebenone delays the onset of cardiac functional alteration without correction of Fe-S enzymes deficit in a mouse model for Friedreich ataxia. *Hum. Mol. Genet.* **13,** 1017–1024
22. Gardin, J. M., Siri, F. M., Kitsis, R. N., Edwards, J. G., and Leinwand, L. A. (1995) Echocardiographic assessment of left ventricular mass and systolic function in mice. *Circ. Res.* **76,** 907–914
23. Manning, W. J., Wei, J. Y., Katz, S. E., Litwin, S. E., and Douglas, P. S. (1994) *In vivo* assessment of LV mass in mice using high-frequency cardiac ultrasound: necropsy validation. *Am. J. Physiol.* **266,** H1672–1675
24. Jakobsen, C. J., Torp, P., and Sloth, E. (2006) Assessment of left ventricular ejection fraction may invalidate the reliability of EuroSCORE. *Eur. J. Cardiothorac. Surg.* **29,** 978–982
25. Garratt, A. N., Voiculescu, O., Topilko, P., Charnay, P., and Birchmeier, C. (2000) A dual role of erbB2 in myelination and in expansion of the schwann cell precursor pool. *J. Cell Biol.* **148,** 1035–1046
26. Kober, F., Iltis, I., Cozzone, P. J., and Bernard, M. (2005) Myocardial blood flow mapping in mice using high-resolution spin labeling magnetic resonance imaging: influence of ketamine/xylazine and isoflurane anesthesia. *Magn. Reson. Med.* **53,** 601–606
27. Jacquier, A., Kober, F., Bun, S., Giorgi, R., Cozzone, P. J., and Bernard, M. (2011) Quantification of myocardial blood flow and flow reserve in rats using arterial spin labeling MRI: comparison with a fluorescent microsphere technique. *NMR Biomed.* **24,** 1047–1053
28. Matz, R. L., de Sotomayor, M. A., Schott, C., Stoclet, J. C., and Andriantsitohaina, R. (2000) Vascular bed heterogeneity in age-related endothelial dysfunction with respect to NO and eicosanoids. *Br. J. Pharmacol.* **131,** 303–311
29. Warren, C. M., Krzesinski, P. R., and Greaser, M. L. (2003) Vertical agarose gel electrophoresis and electroblotting of high-molecular-weight proteins. *Electrophoresis* **24,** 1695–1702
30. Gautel, M., Goulding, D., Bullard, B., Weber, K., and Fürst, D. O. (1996) The central Z-disk region of titin is assembled from a novel repeat in variable. *J. Cell Sci.* **109,** 2747–2754
31. Shen, Z., Li, C., Frieler, R. A., Gerasimova, A. S., Lee, S. J., Wu, J., Wang, M. M., Lumeng, C. N., Brosius, F. C., 3rd, Duan, S. Z., and Mortensen, R. M. (2012) Smooth muscle protein 22 α-Cre is expressed in myeloid cells in mice. *Biochem. Biophys. Res. Commun.* **422,** 639–642
32. Savolainen, S. M., Foley, J. F., and Elmore, S. A. (2009) Histology atlas of the developing mouse heart with emphasis on E11.5 to E18.5. *Toxicol. Pathol.* **37,** 395–414
33. Woldt, E., Matz, R. L., Terrand, J., Mlih, M., Gracia, C., Foppolo, S., Martin, S., Bruban, V., Ji, J., Velot, E., Herz, J., and Boucher, P. (2011) Differential signaling by adaptor molecules LRP1 and ShcA regulates adipogenesis by the insulin-like growth factor-1 receptor. *J. Biol. Chem.* **286,** 16775–16782
34. Tskhovrebova, L., and Trinick, J. (2003) Titin: properties and family relationships. *Nat. Rev. Mol. Cell Biol.* **4,** 679–689
35. Pyle, W. G., and Solaro, R. J. (2004) At the crossroads of myocardial signaling: the role of Z-discs in intracellular signaling and cardiac function. *Circ. Res.* **94,** 296–305
36. Epstein, N. D., and Davis, J. S. (2003) Sensing stretch is fundamental. *Cell* **112,** 147–150
37. Odiete, O., Hill, M. F., and Sawyer, D. B. (2012) Neuregulin in cardiovascular development and disease. *Circ. Res.* **111,** 1376–1385
38. Jiang, Z., and Zhou, M. (2010) Neuregulin signaling and heart failure. *Curr. Heart Fail. Rep.* **7,** 42–47
39. Moncman, C. L., and Wang, K. (1995) Nebulette: a 107 kDa nebulin-like

protein in cardiac muscle. *Cell Motil. Cytoskeleton* **32,** 205–225
40. Maiellaro-Rafferty, K., Wansapura, J. P., Mendsaikhan, U., Osinska, H., James, J. F., Taylor, M. D., Robbins, J., Kranias, E. G., Towbin, J. A., and Purevjav, E. (2013) Altered regional cardiac wall mechanics are associated with differential cardiomyocyte calcium handling due to nebulette mutations in preclinical inherited dilated cardiomyopathy. *J. Mol. Cell. Cardiol.* **60,** 151–160
41. Purevjav, E., Varela, J., Morgado, M., Kearney, D. L., Li, H., Taylor, M. D., Arimura, T., Moncman, C. L., McKenna, W., Murphy, R. T., Labeit, S., Vatta, M., Bowles, N. E., Kimura, A., Boriek, A. M., and Towbin, J. A. (2010) Nebulette mutations are associated with dilated cardiomyopathy and endocardial fibroelastosis. *J. Am. Coll. Cardiol.* **56,** 1493–1502
42. Granzier, H. L., and Labeit, S. (2004) The giant protein titin: a major player in myocardial mechanics, signaling, and disease. *Circ. Res.* **94,** 284–295
43. Gerull, B., Gramlich, M., Atherton, J., McNabb, M., Trombitás, K., Sasse-Klaassen, S., Seidman, J. G., Seidman, C., Granzier, H., Labeit, S., Frenneaux, M., and Thierfelder, L. (2002) Mutations of TTN, encoding the giant muscle filament titin, cause familial dilated cardiomyopathy. *Nat. Genet.* **30,** 201–204
44. Guo, W., Schafer, S., Greaser, M. L., Radke, M. H., Liss, M., Govindarajan, T., Maatz, H., Schulz, H., Li, S., Parrish, A. M., Dauksaite, V., Vakeel, P., Klaassen, S., Gerull, B., Thierfelder, L., Regitz-Zagrosek, V., Hacker, T. A., Saupe, K. W., Dec, G. W., Ellinor, P. T., MacRae, C. A., Spallek, B., Fischer, R., Perrot, A., Özcelik, C., Saar, K., Hubner, N., and Gotthardt, M. (2012) RBM20, a gene for hereditary cardiomyopathy, regulates titin splicing. *Nat. Med.* **18,** 766–773
45. Radke, M. H., Peng, J., Wu, Y., McNabb, M., Nelson, O. L., Granzier, H., and Gotthardt, M. (2007) Targeted deletion of titin N2B region leads to diastolic dysfunction and cardiac atrophy. *Proc. Natl. Acad. Sci. U.S.A.* **104,** 3444–3449
46. Herman, D. S., Lam, L., Taylor, M. R., Wang, L., Teekakirikul, P., Christodoulou, D., Conner, L., DePalma, S. R., McDonough, B., Sparks, E., Teodorescu, D. L., Cirino, A. L., Banner, N. R., Pennell, D. J., Graw, S., Merlo, M., Di Lenarda, A., Sinagra, G., Bos, J. M., Ackerman, M. J., Mitchell, R. N., Murry, C. E., Lakdawala, N. K., Ho, C. Y., Barton, P. J., Cook, S. A., Mestroni, L., Seidman, J. G., and Seidman, C. E. (2012) Truncations of titin causing dilated cardiomyopathy. *New Engl. J. Med.* **366,** 619–628
47. Zhao, Y. Y., Liu, Y., Stan, R. V., Fan, L., Gu, Y., Dalton, N., Chu, P. H., Peterson, K., Ross, J., Jr., and Chien, K. R. (2002) Defects in caveolin-1 cause dilated cardiomyopathy and pulmonary hypertension in knockout mice. *Proc. Natl. Acad. Sci. U.S.A.* **99,** 11375–11380
48. Sebestyén, M. G., Wolff, J. A., and Greaser, M. L. (1995) Characterization of a 5.4 kb cDNA fragment from the Z-line region of rabbit cardiac titin reveals phosphorylation sites for proline-directed kinases. *J. Cell Sci.* **108,** 3029–3037
49. Sharma, P., Ghavami, S., Stelmack, G. L., McNeill, K. D., Mutawe, M. M., Klonisch, T., Unruh, H., and Halayko, A. J. (2010) β-Dystroglycan binds caveolin-1 in smooth muscle: a functional role in caveolae distribution and Ca^{2+} release. *J. Cell Sci.* **123,** 3061–3070
50. Kaufman, M. H., and Navaratnam, V. (1981) Early differentiation of the heart in mouse embryos. *J. Anat.* **133,** 235–246
51. Vasti, C., Witt, H., Said, M., Sorroche, P., García-Rivello, H., Ruiz-Noppinger, P., and Hertig, C. M. (2012) Doxorubicin and NRG-1/erbB4-deficiency affect gene expression profile: involving protein homeostasis in mouse. *ISRN Cardiol.* **2012**, 745185
52. Lemmens, K., Doggen, K., and De Keulenaer, G. W. (2007) Role of neuregulin-1/ErbB signaling in cardiovascular physiology and disease: implications for therapy of heart failure. *Circulation* **116,** 954–960
53. Sawyer, D. B., and Caggiano, A. (2011) Neuregulin-1β for the treatment of systolic heart failure. *J. Mol. Cell. Cardiol.* **51,** 501–505
54. Stevenson, L. E., Ravichandran, K. S., and Frackelton, A. R., Jr. (1999) Shc dominant negative disrupts cell cycle progression in both G_0-G_1 and G_2-M of ErbB2-positive breast cancer cells. *Cell Growth Differ.* **10,** 61–71
55. Campreciós, G., Lorita, J., Pardina, E., Peinado-Onsurbe, J., Soley, M., and Ramírez, I. (2011) Expression, localization, and regulation of the neuregulin receptor ErbB3 in mouse heart. *J. Cell Physiol.* **226,** 450–455
56. Zhao, Y. Y., Sawyer, D. R., Baliga, R. R., Opel, D. J., Han, X., Marchionni, M. A., and Kelly, R. A. (1998) Neuregulins promote survival and growth of cardiac myocytes: persistence of ErbB2 and ErbB4 expression in neonatal and adult ventricular myocytes. *J. Biol. Chem.* **273,** 10261–10269
57. Erickson, S. L., O'Shea, K. S., Ghaboosi, N., Loverro, L., Frantz, G., Bauer, M., Lu, L. H., and Moore, M. W. (1997) ErbB3 is required for normal cerebellar and cardiac development: a comparison with ErbB2-and heregulin-deficient mice. *Development* **124,** 4999–5011
58. Russell, B., Curtis, M. W., Koshman, Y. E., and Samarel, A. M. (2010) Mechanical stress-induced sarcomere assembly for cardiac muscle growth in length and width. *J. Mol. Cell. Cardiol.* **48,** 817–823
59. Das, M., Subbayya Ithychanda, S., Qin, J., and Plow, E. F. (2014) Mechanisms of talin-dependent integrin signaling and crosstalk. *Biochim. Biophys. Acta* **1838,** 579–588
60. Cohen, A. W., Park, D. S., Woodman, S. E., Williams, T. M., Chandra, M., Shirani, J., Pereira de Souza, A., Kitsis, R. N., Russell, R. G., Weiss, L. M., Tang, B., Jelicks, L. A., Factor, S. M., Shtutin, V., Tanowitz, H. B., and Lisanti, M. P. (2003) Caveolin-1 null mice develop cardiac hypertrophy with hyperactivation of p42/44 MAP kinase in cardiac fibroblasts. *Am. J. Physiol. Cell Physiol.* **284,** C457–C474